CloudCT 3D volumetric tomography: Considerations for imager preference, comparing visible light, short-wave infrared, and polarized imagers

Masada Tzabari[a], Vadim Holodovsky[a], Omer Shubi[a], Eshkol Eytan[b], Orit Altaratz[b], Ilan Koren[b], Anna Aumann[c], Klaus Schilling[c], and Yoav Y. Schechner[a]

[a]The Viterbi Faculty of Electrical and Computer Engineering, Technion - Israel Institute of Technology, Haifa, Israel
[b]The Department of Earth and Planetary Sciences, The Weizmann Institute of Science, Rehovot, Israel
[c]Zentrum für Telematik e.V., Würzburg, Germany

ABSTRACT

The CloudCT project is a mission that aims to demonstrate 3D volumetric scattering tomography of clouds. A formation of ten nanosatellites will simultaneously image cloud fields from multiple directions, at $\approx 20m$ nadir ground resolution. Based on this data, scattering tomography will seek the 3D volumetric distribution of cloud properties. We quantitatively compare visible polarized imagers to other imagers considered for the mission. We investigated specifically visible light and short-wave infra-red imagers. Each possibility was considered using Large Eddy Simulation clouds. Major consideration criteria are tomographic quality in the face of sensor and photon noise, calibration errors and stray light. We check the sensitivity to unknown stray light and uncertainty in gain calibration.

Keywords: 3D scattering tomography, Polarization, Space-borne imagery

1. INTRODUCTION

Global space-born observations of earth are critically significant to prediction, tracking, and analysis of climate change.

Currently, pressing questions of earth observation are concerned with the uncertainty of climate change.[1,2] One contribution to the uncertainty is due to the modeling of cloud radiation transfer. Cloud coverage accounts for approximately two thirds of the earth system albedo. However, current modeling of cloud radiative transfer has deficiencies, especially regarding small warm clouds. Most atmospheric radiative transfer models applied today rely on the assumption of a 1D plane-parallel atmosphere. This assumption works well enough for atmospheric conditions that are relatively homogeneous laterally. However, clouds, especially small ones, introduce high horizontal inhomogeneity. 3D modeling, as planned for the CloudCT mission, is required.[3–7]

The CloudCT project, funded by the ERC, is a mission that aims to demonstrate 3D volumetric scattering tomography of clouds. A formation of ten cooperating nano-satellites is planned. These will image cloud fields simultaneously from multiple directions, at about 20m nadir resolution. The images will be used in passive 3D scattering computed tomography (CT), based on a 3D radiative transfer model.* Retrieval is based on optimization, fitting modeled images of the cloud to the measurements.[8–14]

We are motivated by previous works in the field of remote sensing of aerosols and clouds. Levis et al.[9] show cloud microphysics retrieval with the AirMSPI instrument,[15] using visible and near-infrared channels. Polarized remote sensing [15–17] show advantage both to aerosol retrieval[18] and clouds.[19–21] Joint and simultaneous imaging with visible, near-infrared and SWIR channels is also used to retrieve cloud optical properties (based on 1D

Further author information: (Send correspondence to M.T.)
M.T.: E-mail: Masada.tz@campus.technion.ac.il, Telephone: +972 77 887 4720
*We use the Spherical Harmonic Discrete Ordinate Method (SHDOM) for 3D radiative transfer.

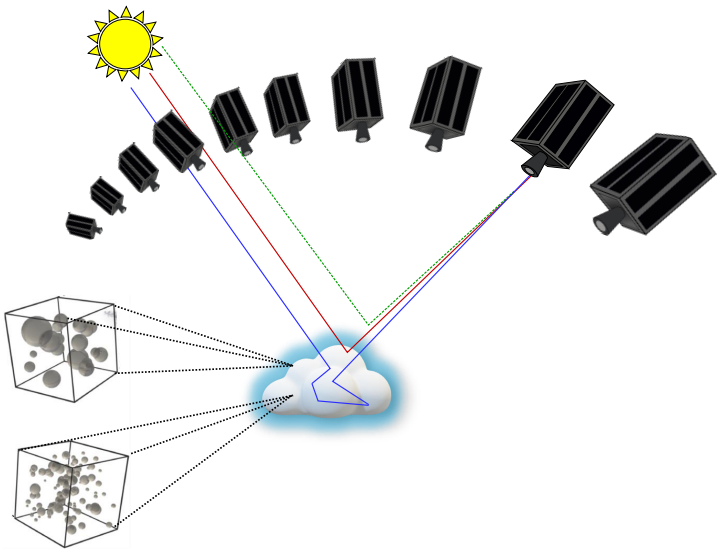

Figure 1. The CloudCT satellite setup for scattering computed tomography.

atmosphere assumption). This idea was first developed by [22] and is currently used for cloud retrieval by the MODIS instrument.[23]

The choice of an imager is of importance. We present considerations regarding polarized visible (POL), unpolarized visible (VIS), and unpolarized short-wave infra-red (SWIR) imagers. We present simulation results for overall retrieval quality, comparing a few practical imager setup configurations. These take into account the limitations of the different imagers. We also present a comparison of the effect of uncertainties on retrieval quality. We consider uncertain stray light and random gain.

2. IMAGER CONSIDERATIONS

Here we point out some of the considerations:

1. *Volume*: The platforms used in the formation are 3U CubeSat satellites ($\approx 10 \times 10 \times 30$ $\left[\text{cm}^3\right]$). The volume dedicated to the imager payload must be smaller than a liter.

2. *Signal to noise ratio (SNR)*: For reasonably high SNR, pixels should have sufficient full well and the camera dark noise should be reasonably low. These two issues are discussed here. Regarding the full well, the signal gathered by a pixel is proportional to the pixel area, exposure time, spectral waveband and squared lens diameter. The limited volume constrains the lens diameter, and in turn, the resolvable features in the atmosphere. The exposure time and spectral waveband width need to be wide, while meeting other constraints that we detail. The second issue is the camera noise, particularly dark current noise. It depends on the type of sensor, exposure time, and the temperature of the sensor. SWIR sensors can generate significantly more dark current noise than modern silicon-based VIS sensors. To have a high SNR, the SWIR sensor should be cooled and thermally stabilized. Thus, it requires on-board cooling. This is a complication, due to the limited resources of our platforms.

3. *Calibration*: Due to the limited volume dedicated to the payload, in-orbit calibration is restricted to vicarious methods. In addition to standard calibration required for remote sensing, POL imagers require additional polarimetric calibration.

4. *Resolution*: High spatial resolution is required for analysis of small clouds. The prefered Ground Sampling Distance (GSD) is ≈ 20 [m] at Nadir. Due to diffraction, longer wavelengths require larger optics. In

addition, large pixels also require large optics. Current SWIR sensors which have space heritage are of pixels no smaller than $\approx 15 \times 15$ $[\mu m^2]$. Thus, the GSD of a SWIR imager is limited by our volume constraint. In spite of our preference, in SWIR simulations the GSD is restricted to 50 [m] at Nadir.

5. *Waveband*: Basic considerations for waveband choice are signal contrast and intensity. In VIS, molecular scattering biases the cloud signal (of both intensity and polarization). This increases photon noise, without increasing the signal of interest. This effect increases at shorter wavelengths. On the other hand, solar irradiance and quantum efficiency (QE) decrease at long wavelengths. As a midway between these effects, the visible waveband in the current simulations is between 620 [nm] and 670 [nm]. In SWIR, sensitivity to microphysics increases at longer wavelengths.[22] However, in an InGaAs sensor, the typical QE is restricted to ≈ 1700 [nm]. In addition, a sufficient signal to noise ratio requires high atmospheric transmittance. Due to these considerations, the SWIR waveband considered is between 1628 [nm] and 1658 [nm].

6. *Field Of View (FOV)*: The FOV should allow a coverage of cloud fields yielding significant statistical information. In addition, for multi-view imaging, the FOV must be wide enough to ensure a significant overlap between the images, despite random errors in the attitude settings of the platforms. The FOV of the VIS is $\sim 49 \times 41$ $[km^2]$ on the ground at nadir. However, in current simulations which retrieve single clouds, the rendered field is less than $\sim 1 \times 1$ $[km^2]$.

7. *Exposure time*: Let S be the velocity of the satellites. To avoid motion blur of more than a pixel GSD, it is important that the exposure time Δt satisfy:

$$\Delta t \leq \frac{\mathrm{GSD}}{S}. \tag{1}$$

   For example, at orbital altitude of $\sim$500 [km], the velocity is $\approx$7.612 [km/sec]. Thus $\Delta t \leq \frac{0.02}{7.612} \approx 2.6$ [msec].

8. *Space compatibility*: Off-the-shelf space-suitable imagers for CubeSats have significant advantages, particularly in low-budget missions having a short time-scale for planning. There are several VIS cameras having space heritage, which may be suitable for the mission requirements. Currently, though there are SWIR and POL cameras for CubeSats,[24,25] they do not fulfill the requirements. Suitable cameras will need to be hardened for the space environment.

9. *Retrieval quality*: The retrieval quality resulting from different setups, within the constraints of the mission, are assessed by simulations. A comparison is presented in this paper, showing an advantage of POL imagers.

10. *Susceptibility to uncertainties*: The retrieval quality is further assessed, under conditions of random gain uncertainty and effects of stray light. A comparison is presented in this paper, showing an advantage of POL imagers.

We found that the constraints limiting SWIR imagers are significant, while the performance does not clearly justify the investment. Therefor, from here on, we present only comparisons of VIS and POL setups.

3. IMAGER SETUP

The satellites' configuration is constant in all demonstrations. Ten satellites are assumed to be in a trailing formation (*string of pearls*), moving northward consecutively. The orbit altitude is 500 [km]. The uniform distance between each pair of nearest-neighbor satellites is 100 [km] (on orbit arc). The span of the satellites' viewing angles is 85°, with the middle satellite near nadir. The simulated pose of the Sun is to the east, 25° from the zenith. We considered three cases of imager setups.

1. VIS: Each satellite has a single VIS imager.

2. POL: Each satellite has a single POL imager.

3. POL + scan: Each satellite has a single POL imager. The scattering angles between 135° and 165° are known as the *cloudbow*. In this region, the polarization of scattered light is highly sensitive to the cloud microphysics.[19,26,27] In this setup, an additional cloudbow scan of eight views is acquired by one of the imagers. The acquisition time depends on the viewing angle of the imager and may reach 30 [sec]. Considering cloud dynamics, this can be an acceptable time scale.[14]

Each imager used for the current demonstrations is simulated according to its specifications. The POL camera is simulated using specifications of the Sony IMX250MZR sensor.[28] The sensor has grid-wire polarizing filters which are formed on the chip. Each block of four pixels has four filter axes [0°,45°,90°,135°], relative to the sensor's horizontal axis (See Fig. 2). Using such imagers, the Stokes vector is calculated either per block, or per pixel by means of demosaicing. In the latter, the missing information in each pixel is estimated by interpolation. For this demonstration, we assume ideal demosaicing.

4. RETRIEVAL METHOD

The retrieval uses the pySHDOM[29] method developed by Levis et al.[9,11] These works introduce 3D scattering computed tomography, based on the Spherical Harmonic Discrete Ordinate Method (SHDOM) for radiative-transfer.[30] The method retrieves cloud properties by optimization, fitting multi-view images to a physics based forward-model. This is a generalization of CT to recover scatterers by passive sensing, relying only on the Sun as an illumination source. The method was further developed using vSHDOM,[31] for vectorized radiative-transfer, allowing consideration of polarization. In this method, cloud properties are retrieved by fitting Stokes vectors.

Cloud properties within the field are defined according to Large-Eddy Simulations (LES)[32] based on the Barbados Oceanographic and Meteorology Experiment (BOMEX). The LES data is pre-computed and serves as ground-truth for the simulations. In this demonstration, a set of six separate cloud cells are chosen from the BOMEX data-set. Data acquisition is then simulated. Images are rendered using each imager model, including photon noise, read noise, dark current noise, and quantization noise.

4.1 Parameter definition

For small warm clouds, we assume spherical droplets. Let a droplet radius be r. Let the droplet size distribution at a volume element be $n(r)$ $\left[\frac{1}{\mu\mathrm{m}}\cdot\frac{1}{m^2}\right]$. An effective radius r_e $[\mu\mathrm{m}]$ and a unitless effective variance v_e are defined[33] by:

$$r_\mathrm{e}=\frac{\int(\pi r^2)rn(r)\mathrm{d}r}{\int(\pi r^2)n(r)\mathrm{d}r},\quad v_\mathrm{e}=\frac{\int\left(r-r_\mathrm{e}\right)^2(\pi r^2)n(r)\mathrm{d}r}{r_\mathrm{e}^2\int(\pi r^2)n(r)\mathrm{d}r}. \tag{2}$$

The 3D distribution of the liquid water content (LWC) is

$$\mathrm{LWC}=\frac{4}{3}\pi\rho_\mathrm{w}\int_r r^3n(r)\mathrm{d}r\qquad\left[\frac{\mathrm{g}}{\mathrm{m}^3}\right], \tag{3}$$

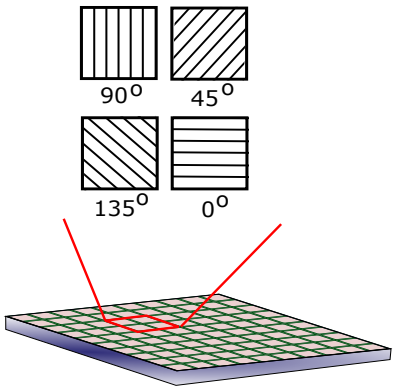

Figure 2. Wire-grid polarizing filters in a block of pixels in Sony Polarsens sensor.

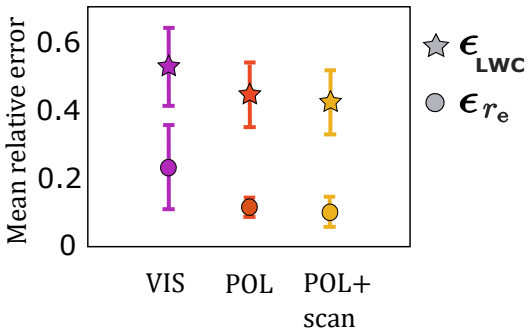

Figure 3. Quantitative comparison of retrieval mean relative errors ϵ_{LWC} and ϵ_{r_e}, for the different setups considered.

where $\rho_w = 1\ \left[\frac{g}{cm^3}\right]$ is the water density. In the chosen set of simulated clouds, the mean value of r_e per cloud is between 6.2 [μm] and 10 [μm]. LWC values reach up to 2 $\left[\frac{g}{m^3}\right]$. This demonstration focuses on retrieval of LWC and r_e as in 34. The initialization of the optimization uses parametrized vertical profiles of LWC and r_e. The parameters are found by a preliminary optimization process.[35] Therefore, the initialization also depends on the imager setup.

5. RETRIEVAL QUALITY COMPARISON

5.1 Retrieval quality measure

Let $\mathbf{LWC}$ and $\boldsymbol{r}_e$ be the ground-truth fields of the estimated 3D fields $\hat{\mathbf{LWC}}$ and $\hat{\boldsymbol{r}_e}$. The quality of a retrieval is quantitatively assessed by relative error ϵ:[34]

$$\epsilon_{\mathrm{LWC}} = \frac{\|\hat{\mathbf{LWC}} - \mathbf{LWC}\|_1}{\|\mathbf{LWC}\|_1}, \quad \epsilon_{r_e} = \frac{\|\hat{\mathbf{r}_e} - \boldsymbol{r}_e\|_1}{\|\boldsymbol{r}_e\|_1}. \tag{4}$$

The mean relative errors of the cloud-set are compared in Fig. 3. The POL setup has a significant advantage over VIS, particularly for retrieving r_e. The cloudbow scan gives an additional advantage to the POL setup.

5.2 Consequences of gain errors and stray light

In order to quantify susceptibility of the different considered imagers, uncertainties are introduced to the calibration. Two random effects are considered: stray light and per-pixel gain uncertainty.

Out of the overall FOV, the pixels comprising a single cloud cell are clustered, where each cluster has rather a few pixels. Therefore, stray light is considered spatially uniform over the pixels used for tomography of a single cloud. We consider stray light to be a random value for each imager in the setup. For each imager, the stray light is randomly sampled from a uniform distribution defined between 0% and 5% of the mean intensity of the image.

The gain uncertainty is defined per pixel. The relative change in gain is randomly sampled from a normal distribution with standard deviation of 5%. For the polarized imagers, random gain uncertainty is applied per sensor pixel, prior to the Stokes vector calculation. Note that the values used for this demonstration are drastically higher than standard requirements. These are used to simplify the susceptibility comparison of the considered setups.

Let ϵ' be the relative error of a retrieval which is affected by one of these said uncertainties. For each effect, the consequent change to a cloud retrieval is quantified as:

$$\Delta\epsilon_{\mathrm{LWC}} = \epsilon'_{\mathrm{LWC}} - \epsilon_{\mathrm{LWC}}\ , \quad \Delta\epsilon_{r_e} = \epsilon'_{r_e} - \epsilon_{r_e}. \tag{5}$$

As presented in Fig. 4, the change in relative error due to stray light is up to 0.05 for both ϵ_{LWC} and ϵ_{r_e}. The VIS setup is affected much more than the POL setup.

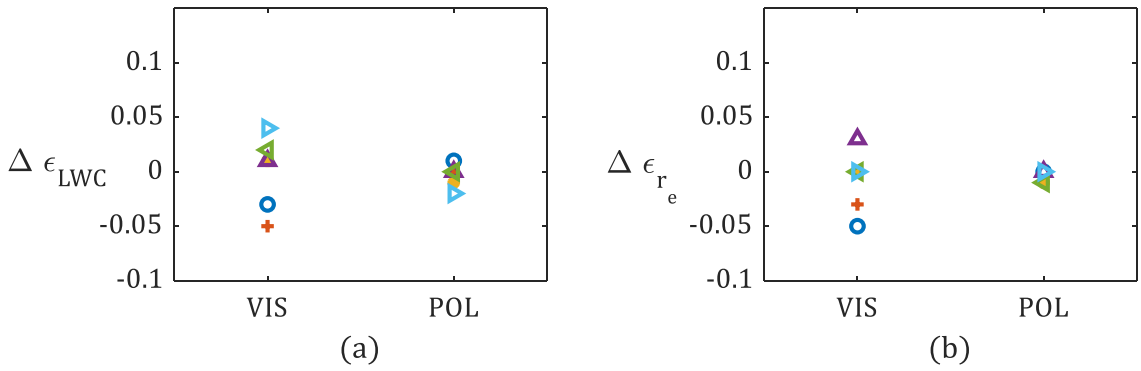

Figure 4. The change in retrieval relative errors (a) ϵ_{LWC} and (b) $\epsilon_{r_{\mathrm{e}}}$, when introducing a uniform uncertain random stray light. Different colors represent different clouds.

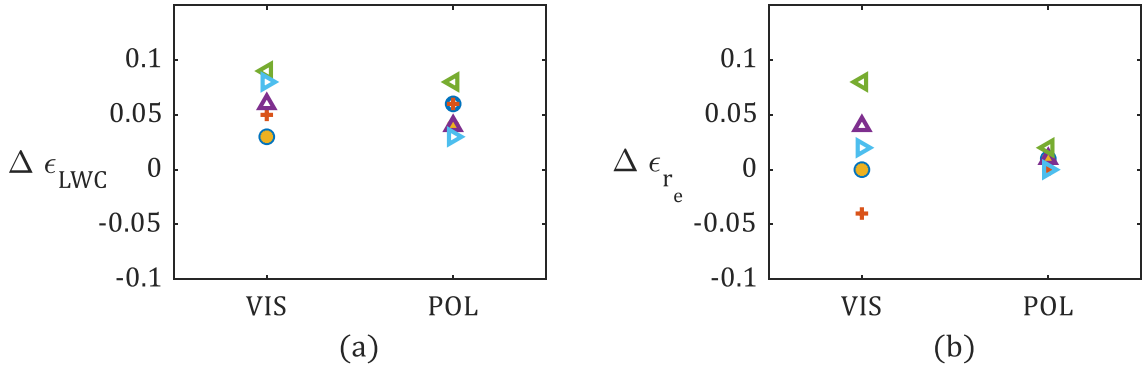

Figure 5. The change in retrieval relative errors (a) ϵ_{LWC} and (b) $\epsilon_{r_{\mathrm{e}}}$, when introducing a uniform uncertain random gain. Different colors represent different clouds.

The change in relative error due to gain uncertainty is presented in Fig. 5. In the retrieval of the LWC, the consequence of gain uncertainty is more significant than that of stray light, with a similar effect on both setups. However, in retrieval of r_{e}, the POL setup is much less sensitive to this uncertainty. This finding is significant and nontrivial. In POL imagers, Stokes vector components are calculated relying on four radiance values (see Sec. 3). In the simulations, each of these values has a different random and uncertain gain. While in VIS each pixel is affected individually, in POL the Stokes vectors are affected by a combined uncertainty. Nevertheless, the POL setup seems numerically more robust than the VIS setup.

We find through this comparison a significant advantage to the use of a POL setup for the CloudCT mission. Within the constraints of the mission, we find this to be a preferable setup. Even so, we are aware of the additional complexity included in such a setup, such as in-orbit vicarious calibration.

6. CONCLUSION

We present an overall glance at the process of payload choice for CloudCT. This comprises many constraints and considerations. We considered VIS, SWIR, and POL imagers. From these, the POL setup appears to be most suitable within the mission constraints, due to retrieval results and stability to both stray light and gain uncertainties.

ACKNOWLEDGMENTS

We are grateful to Anthony Davis, Dave Diner and Linda Forster for useful discussions and good advice. We thank Aviad Levis and Jesse Loveridge for the pySHDOM code, useful discussions and being responsive to questions. We thank Miri Haramati, Johanan Erez, Ina Talmon and Daniel Yagodin for technical support. Yoav Schechner is the Mark and Diane Seiden Chair in Science at the Technion. He is a Landau Fellow - supported by the Taub Foundation. His work was conducted in the Ollendorff Minerva Center. Minvera is funded through the BMBF. This project has received funding from the European Union's Horizon 2020 research and innovation program under grant agreement No 810370-ERC-CloudCT.

REFERENCES

[1] Bony, S. and Dufresne, J.-L., "Marine boundary layer clouds at the heart of tropical cloud feedback uncertainties in climate models," *Geophys. Res. Lett.* **32**(20) (2005).

[2] Gettelman, A. and Sherwood, S., "Processes responsible for cloud feedback," *Curr. Clim. Change Rep.* **2**(4), 179–189 (2016).

[3] Davis, A., Marshak, A., Cahalan, R., and Wiscombe, W., "The landsat scale break in stratocumulus as a three-dimensional radiative transfer effect: Implications for cloud remote sensing," *J. Atmos. Sci.* **54**(2), 241–260 (1997).

[4] Várnai, T. and Marshak, A., "Statistical analysis of the uncertainties in cloud optical depth retrievals caused by three-dimensional radiative effects," *J. Atmos. Sci.* **58**(12), 1540–1548 (2001).

[5] Zinner, T. and Mayer, B., "Remote sensing of stratocumulus clouds: Uncertainties and biases due to inhomogeneity," *J. Geophys. Res. Atmos.* **111**(D14) (2006).

[6] Forster, L., Davis, A. B., Diner, D. J., and Mayer, B., "Toward cloud tomography from space using MISR and MODIS: Locating the "veiled core" in opaque convective clouds," *J. Atmos. Sci.* **78**(1), 155–166 (2021).

[7] Loveridge, J. and Davies, R., "Cloud heterogeneity in the marine midlatitudes: Dependence on large-scale meteorology and implications for general circulation models," *J Geophys Res Atmos* **124**(6), 3448–3463 (2019).

[8] Aides, A., Schechner, Y. Y., Holodovsky, V., Garay, M. J., and Davis, A. B., "Multi sky-view 3D aerosol distribution recovery," *Opt. Express* **21**(22), 25820–25833 (2013).

[9] Levis, A., Schechner, Y. Y., Aides, A., and Davis, A. B., "Airborne three-dimensional cloud tomography," in [*ICCP*], 3379–3387, IEEE (2015).

[10] Holodovsky, V., Schechner, Y. Y., Levin, A., Levis, A., and Aides, A., "In-situ multi-view multi-scattering stochastic tomography," in [*ICCP*], 1–12, IEEE (2016).

[11] Levis, A., Schechner, Y. Y., and Davis, A. B., "Multiple-scattering microphysics tomography," in [*CVPR*], IEEE (July 2017).

[12] Loeub, T., Levis, A., Holodovsky, V., and Schechner, Y. Y., "Monotonicity prior for cloud tomography," in [*ECCV*], 24–29, Springer (2020).

[13] Aides, A., Levis, A., Holodovsky, V., Schechner, Y. Y., Althausen, D., and Vainiger, A., "Distributed sky imaging radiometry and tomography," in [*ICCP*], 1–12, IEEE (2020).

[14] Ronen, R., Schechner, Y. Y., and Eytan, E., "Spatiotemporal tomography based on scattered multiangular signals and its application for resolving evolving clouds using moving platforms," *arXiv preprint arXiv:2012.03223* (2020).

[15] Diner, D. J., Xu, F., Garay, M. J., Martonchik, J. V., Rheingans, B. E., Geier, S., Davis, A., Hancock, B., Jovanovic, V., Bull, M., et al., "The airborne multiangle spectropolarimetric imager (AirMSPI): a new tool for aerosol and cloud remote sensing," *Atmos. Meas. Tech.* **6**(8), 2007–2025 (2013).

[16] Tyo, J. S., Goldstein, D. L., Chenault, D. B., and Shaw, J. A., "Review of passive imaging polarimetry for remote sensing applications," *Appl. Opt.* **45**(22), 5453–5469 (2006).

[17] Snik, F., Craven-Jones, J., Escuti, M., Fineschi, S., Harrington, D., De Martino, A., Mawet, D., Riedi, J., and Tyo, J. S., "An overview of polarimetric sensing techniques and technology with applications to different research fields," in [*Polarization: measurement, analysis, and remote sensing XI*], **9099**, 90990B, International Society for Optics and Photonics (2014).

[18] Emde, C., Buras, R., Mayer, B., and Blumthaler, M., "The impact of aerosols on polarized sky radiance: model development, validation, and applications," *Atmospheric Chem. Phys.* **10**(2), 383–396 (2010).

[19] Xu, F., van Harten, G., Diner, D. J., Davis, A. B., Seidel, F. C., Rheingans, B., Tosca, M., Alexandrov, M. D., Cairns, B., Ferrare, R. A., et al., "Coupled retrieval of liquid water cloud and above-cloud aerosol properties using the airborne multiangle spectropolarimetric imager (AirMSPI)," *J. Geophys. Res. Atmos.* **123**(6), 3175–3204 (2018).

[20] Parol, F., Buriez, J.-C., Vanbauce, C., Riédi, J., Doutriaux-Boucher, M., Vesperini, M., Sèze, G., Couvert, P., Viollier, M., Bréon, F., et al., "Review of capabilities of multi-angle and polarization cloud measurements from POLDER," *Adv. Space Res.* **33**(7), 1080–1088 (2004).

[21] Breon, F. M. and Goloub, P., "Cloud droplet effective radius from spaceborne polarization measurements," *Geophys. Res. Lett* **25**(11), 1879–1882 (1998).

[22] Nakajima, T. and King, M. D., "Determination of the optical thickness and effective particle radius of clouds from reflected solar radiation measurements. part i: Theory," *J. Atmos. Sci.* **47**(15), 1878–1893 (1990).

[23] Platnick, S., Meyer, K. G., King, M. D., Wind, G., Amarasinghe, N., Marchant, B., Arnold, G. T., Zhang, Z., Hubanks, P. A., Holz, R. E., et al., "The MODIS cloud optical and microphysical products: Collection 6 updates and examples from terra and aqua," *TGRS* **55**(1), 502–525 (2016).

[24] Martins, J. V., Nielsen, T., Fish, C., Sparr, L., Schoeberl, M., and Remer, L., "HARP CubeSat – An innovative Hyperangular Imaging Polarimeter for Earth Science Applications," *Proceedings of the AIAA/USU Conference on Small Satellites* , 29 (2014).

[25] Pack, D. W., Coffman, C., and Santiago, J. R., "A Year in Space for the CUbesat MULtispectral Observing System: CUMULOS," *Proceedings of the AIAA/USU Conference on Small Satellites* (310) (2019).

[26] Alexandrov, M. D., Cairns, B., Emde, C., Ackerman, A. S., and van Diedenhoven, B., "Accuracy assessments of cloud droplet size retrievals from polarized reflectance measurements by the research scanning polarimeter," *Remote Sens. Environ.* **125**, 92–111 (2012).

[27] Alexandrov, M. D., Miller, D. J., Rajapakshe, C., Fridlind, A., van Diedenhoven, B., Cairns, B., Ackerman, A. S., and Zhang, Z., "Vertical profiles of droplet size distributions derived from cloud-side observations by the research scanning polarimeter: Tests on simulated data," *Atmos. Res.* (2020).

[28] "Polarization image sensor with four-directional on-chip polarizer and global shutter function." https://www.sony-semicon.co.jp/e/products/IS/industry/product/polarization.html.

[29] Levis, A., Loveridge, J., and Aides, A., "pySHDOM." https://github.com/aviadlevis/pyshdom (2019).

[30] Evans, K. F., "The spherical harmonics discrete ordinate method for three-dimensional atmospheric radiative transfer," *J. Atmos. Sci.* **55**(3), 429–446 (1998).

[31] Doicu, A., Efremenko, D., and Trautmann, T., "A multi-dimensional vector spherical harmonics discrete ordinate method for atmospheric radiative transfer," *J. Quant. Spectrosc. Radiat. Transf.* **118**, 121–131 (2013).

[32] Khairoutdinov, M. and Randall, D., "SAM." http://rossby.msrc.sunysb.edu/~marat/SAM.html (2003).

[33] Hansen, J. E. and Travis, L. D., "Light scattering in planetary atmospheres," *Space Sci. Rev.* **16**(4), 527–610 (1974).

[34] Levis, A., Schechner, Y. Y., Davis, A. B., and Loveridge, J., "Multi-view polarimetric scattering cloud tomography and retrieval of droplet size," *Remote Sens.* **12**(17), 2831 (2020).

[35] Tzabari, M., Holodovsky, V., Shubi, O., Eshkol, E., and Schechner, Y. Y., "Advances in 3D scattering tomography of cloud micro-physics," *arXiv preprint arXiv:2103.10305* (2021).